# Generalized monotonically convergent algorithms for solving quantum optimal control problems

Cite as: J. Chem. Phys. **120**, 5509 (2004); https://doi.org/10.1063/1.1650297
Submitted: 27 October 2003 . Accepted: 05 January 2004 . Published Online: 12 March 2004

Yukiyoshi Ohtsuki, Gabriel Turinici, and Herschel Rabitz

## ARTICLES

# Generalized monotonically convergent algorithms for solving quantum optimal control problems

Yukiyoshi Ohtsuki[a)]
*Department of Chemistry, Graduate School of Science, Tohoku University, Sendai 980-8578, Japan*

Gabriel Turinici[b)]
*INRIA Rocquencourt, MICMAC Project, Domaine de Voluceau, Rocquencourt B.P. 105, 78153 Le Chesnay Cedex, France and CERMICS-ENPC, Champs sur Marne, 77455 Marne la Vallée Cedex, France*

Herschel Rabitz[c)]
*Department of Chemistry, Princeton University, New Jersey 08544*

(Received 27 October 2003; accepted 5 January 2004)

A wide range of cost functionals that describe the criteria for designing optimal pulses can be reduced to two basic functionals by the introduction of product spaces. We extend previous monotonically convergent algorithms to solve the generalized pulse design equations derived from those basic functionals. The new algorithms are proved to exhibit monotonic convergence. Numerical tests are implemented in four-level model systems employing stationary and/or nonstationary targets in the absence and/or presence of relaxation. Trajectory plots that conveniently present the global nature of the convergence behavior show that slow convergence may often be attributed to ''trapping'' and that relaxation processes may remove such unfavorable behavior.  [DOI: 10.1063/1.1650297]

## I. INTRODUCTION

An optimal control procedure provides a powerful tool for designing a laser pulse to best manipulate molecular dynamics for a specified purpose.[1,2] Recently, Ohtsuki and Rabitz[3] showed that the introduction of product spaces enables the reduction of a wide range of cost functionals that describe the criteria for designing optimal pulses to two basic functionals. The purpose of the present study is to extend the solution algorithms developed by Maday and Turinici[4–6] in order to treat the general pulse design equations derived from those basic functionals. We will prove that the generalized algorithms exhibit monotonic convergence[7–10] and examine their convergence behavior numerically in the presence of dissipation.

Consider a molecule interacting with a time-dependent electric field $E(t)$, and the time evolution is described by the equation of motion:[3]

$$i\hbar \frac{\partial}{\partial t}|u(t)\rangle=[\alpha-\beta E(t)]|u(t)\rangle. \tag{1}$$

Here, the vector $|u(t)\rangle$ specifying a molecular state can be a wave function or a density operator. The radiative interaction is represented by $-\beta E(t)$ and the other field-free interactions are denoted by $\alpha$. The operators, $\alpha$ and $\beta$, can be non-Hermitian.

Using the state vector $|u(t)\rangle$, one of the basic functionals, referred to as type I, is defined by

$$J_{\mathrm{I}}=2\ \mathrm{Re}\langle X|u(t_f)\rangle+2\ \mathrm{Re}\int_0^{t_f}dt\langle Y(t)|u(t)\rangle - \frac{1}{\hbar A}\int_0^{t_f}dt[E(t)]^2, \tag{2}$$

where $\mathrm{Re}\langle X|u(t_f)\rangle$ is the real part of $\langle X|u(t_f)\rangle$, etc. The state vector, $|X\rangle$, specifies a target state at a final time $t_f$ and $|Y(t)\rangle$ denotes a constraint upon the time evolution of intermediate states over the control period. The last term represents the penalty due to pulse fluence, which also steers the optimal pulse away from being singular. In the other functional, referred to as type II, those physical targets and constraints are specified by two Hermitian operators, $X$ and $Y(t)$, so that the functional is expressed as

$$J_{\mathrm{II}}=\langle u(t_f)|X|u(t_f)\rangle+\int_0^{t_f}dt\langle u(t)|Y(t)|u(t)\rangle - \frac{1}{\hbar A}\int_0^{t_f}dt[E(t)]^2. \tag{3}$$

Functional $J_{\mathrm{I}}$ is linear while functional $J_{\mathrm{II}}$ is bilinear with respect to the state vector. Note that the results derived herein can be extended to treat mixtures of those two types as well as cases where the target states are specified by more complex functions.

In our notation, an optimal pulse will maximize a cost functional, and $X$ and $Y(t)$ are suitably defined to be consis-

a)Electronic mail: ohtsuki@mcl.chem.tohoku.ac.jp
b)Electronic mail: gabriel.turinici@inria.fr
c)Electronic mail: hrabitz@princeton.edu

 

tent with this. For example, applying the calculus of variations to Eq. (2) under the constraint of the equation of motion, Eq. (1), we obtain the pulse design equations. The optimal pulse is expressed as

$$E(t) = -A\ \mathrm{Im}\langle \lambda(t)|\beta|u(t)\rangle, \tag{4}$$

where $\mathrm{Im}\langle\lambda(t)|\beta|u(t)\rangle$ is the imaginary part of $\langle\lambda(t)|\beta|u(t)\rangle$. The equation of motion for the Lagrange multiplier associated with the constraint of Eq. (1) is given by

$$i\hbar\frac{\partial}{\partial t}|\lambda(t)\rangle = [\alpha^\dagger - \beta^\dagger E(t)]|\lambda(t)\rangle - i\hbar|Y(t)\rangle \tag{5}$$

with a final condition

$$|\lambda(t_f)\rangle = |X\rangle. \tag{6}$$

In the type II case, we have the same expression for the optimal pulse in Eq. (4). The Lagrange multiplier, however, obeys a different equation of motion given by

$$i\hbar\frac{\partial}{\partial t}|\lambda(t)\rangle = [\alpha^\dagger - \beta^\dagger E(t)]|\lambda(t)\rangle - i\hbar Y(t)|u(t)\rangle \tag{7}$$

with a final condition

$$|\lambda(t_f)\rangle = X|u(t_f)\rangle. \tag{8}$$

In Sec. II, we apply the newly developed algorithm to the above-given general pulse design equations, in which monotonic convergence will be proved. In Sec. III, the convergence behavior is numerically illustrated using few-level models under the influence of dissipation. Numerical efficiencies are examined for several values of the parameters that characterize the iteration algorithms.

## II. SOLUTION ALGORITHM AND ITS CONVERGENCE BEHAVIOR

According to the present iteration algorithm, the pulse design equations at the $k$th step are summarized as follows:

$$i\hbar\frac{\partial}{\partial t}|\lambda^{(k)}(t)\rangle = [\alpha^\dagger - \beta^\dagger \overline{E}^{(k)}(t)]|\lambda^{(k)}(t)\rangle - i\hbar|Y(t)\rangle, \tag{9}$$

with a final condition $|\lambda^{(k)}(t_f)\rangle = |X\rangle$ and

$$i\hbar\frac{\partial}{\partial t}|u^{(k)}(t)\rangle = [\alpha - \beta E^{(k)}(t)]|u^{(k)}(t)\rangle, \tag{10}$$

with an initial condition $|u^{(k)}(0)\rangle = |u_0\rangle$. The electric fields at the $k$th step are given by

$$\overline{E}^{(k)}(t) = (1-\eta_k)E^{(k-1)}(t) - \eta_k A\ \mathrm{Im}\langle\lambda^{(k)}(t)|\beta|u^{(k-1)}(t)\rangle, \tag{11}$$

and

$$E^{(k)}(t) = (1-\zeta_k)\overline{E}^{(k)}(t) - \zeta_k A\ \mathrm{Im}\langle\lambda^{(k)}(t)|\beta|u^{(k)}(t)\rangle, \tag{12}$$

where the parameters, $\zeta_k$, $\eta_k \in [0,2]$, guarantee the monotonic convergence behavior of the algorithm, as shown in the following. This algorithm can start the iteration with either $|u^{(0)}(t)\rangle$ or $|\lambda^{(0)}(t)\rangle$ along with an initial trial field, $E^{(0)}(t)$ or $\overline{E}^{(0)}(t)$.

To investigate the convergence behavior of the algorithm, we consider the case in which the algorithm starts with $E^{(0)}(t)$. The difference in cost functional between the $k$th and $(k-1)$th successive iteration steps is expressed as

$$\begin{aligned}\delta J_{\mathrm{I}}^{(k,k-1)} &= J_{\mathrm{I}}^{(k)} - J_{\mathrm{I}}^{(k-1)} \\ &= 2\ \mathrm{Re}\langle X|\delta u^{(k,k-1)}(t_f)\rangle \\ &\quad + 2\ \mathrm{Re}\int_0^{t_f} dt\langle Y(t)|\delta u^{(k,k-1)}(t)\rangle \\ &\quad - \frac{1}{\hbar A}\int_0^{t_f} dt\{[E^{(k)}(t)]^2 - [E^{(k-1)}(t)]^2\},\end{aligned} \tag{13}$$

where

$$|\delta u^{(k,k-1)}(t)\rangle = |u^{(k)}(t)\rangle - |u^{(k-1)}(t)\rangle. \tag{14}$$

Here we introduce a function, $P^{(k,k-1)}(t) = 2\ \mathrm{Re}\langle\lambda^{(k)}(t)|\delta u^{(k,k-1)}(t)\rangle$. Note that at time $t_f$, $P^{(k,k-1)}(t_f)$ gives the difference in the degree of control achievement associated with the target state, $|X\rangle$, whereas at the initial time, $P^{(k,k-1)}(0) = 0$. Differentiating the function, $P^{(k,k-1)}(t)$, with respect to time, we obtain

$$\begin{aligned}&\frac{d}{dt}P^{(k,k-1)}(t) + 2\ \mathrm{Re}\langle Y(t)|\delta u^{(k,k-1)}(t)\rangle \\ &= -\frac{2}{\hbar}\{\mathrm{Im}\langle\lambda^{(k)}(t)|\beta|u^{(k)}(t)\rangle[E^{(k)}(t) - \overline{E}^{(k)}(t)] \\ &\quad + \mathrm{Im}\langle\lambda^{(k)}(t)|\beta|u^{(k-1)}(t)\rangle[\overline{E}^{(k)}(t) - E^{(k-1)}(t)]\},\end{aligned} \tag{15}$$

where the pulse design equations, Eqs. (9) and (10), are used. Substituting the expressions for the optimal pulses, Eqs. (11) and (12), into Eq. (15), and then integrating both sides of the resulting equation over $t \in [0,t_f]$, we have

$$\begin{aligned}&2\ \mathrm{Re}\langle X|\delta u^{(k,k-1)}(t_f)\rangle + 2\ \mathrm{Re}\int_0^{t_f} dt\langle Y(t)|\delta u^{(k,k-1)}(t)\rangle \\ &= \frac{2}{\hbar A}\int_0^{t_f} dt\Bigg\{[E^{(k)}(t) - \overline{E}^{(k)}(t)]\Bigg[\frac{1}{\zeta_k}E^{(k)}(t) \\ &\quad + \left(1 - \frac{1}{\zeta_k}\right)\overline{E}^{(k)}(t)\Bigg] + [\overline{E}^{(k)}(t) - E^{(k-1)}(t)]\Bigg[\frac{1}{\eta_k}\overline{E}^{(k)}(t) \\ &\quad + \left(1 - \frac{1}{\eta_k}\right)E^{(k-1)}(t)\Bigg]\Bigg\}.\end{aligned} \tag{16}$$

The substitution of Eq. (16) into Eq. (13) yields

$$\begin{aligned}\delta J_{\mathrm{I}}^{(k,k-1)} = \frac{1}{\hbar A}\int_0^{t_f} dt\Bigg\{&\left(\frac{2}{\zeta_k} - 1\right)[E^{(k)}(t) - \overline{E}^{(k)}(t)]^2 \\ &+ \left(\frac{2}{\eta_k} - 1\right)[\overline{E}^{(k)}(t) - E^{(k-1)}(t)]^2\Bigg\}.\end{aligned} \tag{17}$$

Summing both sides of Eq. (17) from $k=1$ to $N$, we can prove the monotonic convergence of the present iteration algorithm, $\delta J_{\mathrm{I}}^{(N,0)}=J_{\mathrm{I}}^{(N)}-J_{\mathrm{I}}^{(0)}\geqslant 0$, provided that the convergence parameters are within $\{\zeta_k,\eta_k\}\in[0,2]$.

We can apply a similar algorithm to type II, the monotonic convergence behavior of which is proved in Appendix A.

## III. NUMERICAL RESULTS

For illustrative purposes, we deal with a simple but frequently employed cost functional:[1,11]

$$J=\langle W(t_f)\rangle-\frac{1}{\hbar A}\int_0^{t_f}dt[E(t)]^2, \tag{18}$$

where an objective is specified by a Hermitian operator, $W$, and the physical significance of the penalty is weighed by a time-independent positive parameter, $A$. This cost functional aims at achieving the largest transition probability from an initial state to an objective state at the target time, $t_f$, while minimizing the pulse fluence.

Consider a system that is surrounded by an optically inactive heat bath,[12] where the system interacts with the field, $E(t)$, through an electric dipole interaction. The system Hamiltonian, $H^t$, specifying the unitary time evolution, consists of a field-free system Hamiltonian, $H_0$, and the interaction potential $-\mu E(t)$, with $\mu$ being the electric dipole moment operator:

$$H^t=H_0-\mu E(t). \tag{19}$$

The system–bath interaction describes nonunitary time evolution, which is approximated by a set of phenomenological relaxation parameters in this study. The time evolution of the system is described by a reduced density operator obtained from the total density operator by taking the trace over all the bath degrees of freedom. Utilizing the double-space (Liouville-space) notation,[11,12] we have the equation of motion for the reduced density operator

$$i\hbar\frac{\partial}{\partial t}|\rho(t)\rangle\rangle=[L_0-ME(t)]|\rho(t)\rangle\rangle-i\hbar\Gamma|\rho(t)\rangle\rangle, \tag{20}$$

where the Liouvillians $L_0$ and $M$ correspond to the commutators, $[H_0,\ldots]$ and $[\mu,\ldots]$, respectively. The (super) operator, $\Gamma$, represents relaxation processes. In this case, the operators $\alpha$ and $\beta$ in Eq. (1) should read $L=L_0-i\hbar\Gamma$ and $M$, respectively. Since the expectation value of the target operator is expressed as $\langle W(t_f)\rangle=\langle\langle W|\rho(t_f)\rangle\rangle$ in the double-space notation, the cost functional in Eq. (18) is reduced to type I.[3,13]

In the following, we will examine the convergence behavior of the algorithms in Sec. II with several values for the convergence parameters, $\zeta$ and $\eta$. We employ four-level systems with stationary and nonstationary targets in the absence or presence of relaxation. Dimensionless energy and time units are used in the calculations. Transition moments are measured in units of $\mu_0$ and denote the electric field strength by the dimensionless energy $\mu_0 E(t)$. The equation of motion in Eq. (20) and that associated with the Lagrange multiplier are expressed in the interaction representation assuming the rotating wave approximation (RWA). These equations are expanded in terms of the eigenstates of $H_0$ and solved by the Runge–Kutta–Fehlberg method. The target time is $t_f=15$ and the interval $0\leqslant t_f\leqslant 15$ is uniformly divided into 9000 time steps.

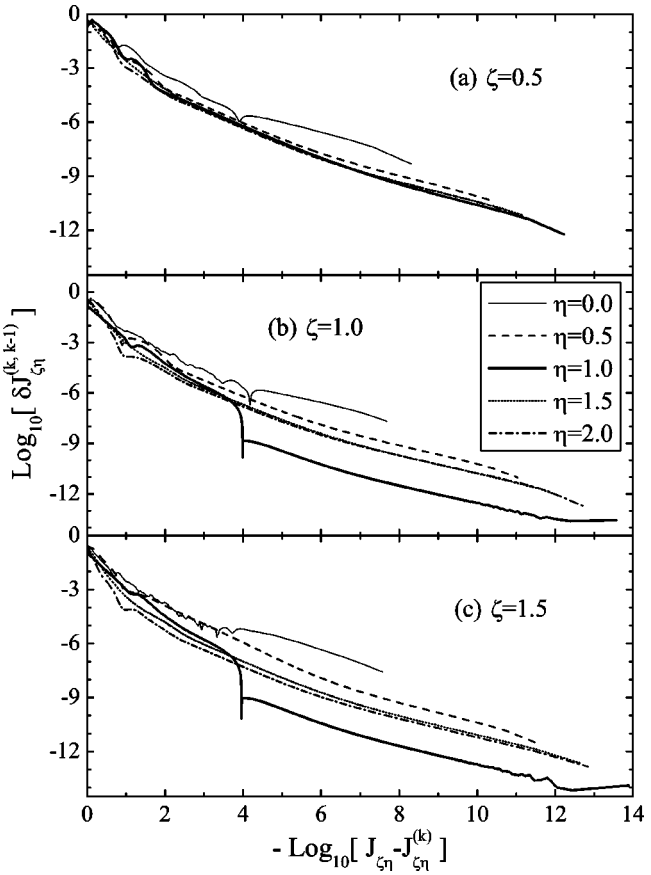


FIG. 1. Global nature of convergence behavior in the absence of relaxation. Three values of (a) $\zeta=0.5$, (b) 1.0, and (c) 1.5 are considered.

We denote the states of the four-level system and their energy eigenvalues by $|n\rangle$ and $\varepsilon_n(n=1,2,3,4)$, respectively. The first model has a symmetrical structure characterized by energy differences $\varepsilon_{31}=30$ and $\varepsilon_{43}=\varepsilon_{32}=20$ ($\varepsilon_{mn}=\varepsilon_m-\varepsilon_n$) and by transition moment elements $\mu_{31}=\mu_{32}=\mu_{43}=\mu_0$ ($\mu_{mn}=\langle m|\mu|n\rangle$). Our purpose is to transfer the initial population in the lowest state, $|1\rangle$, selectively to the $|2\rangle$ state. For this purpose, we employ a target operator, $W=|2\rangle\langle 2|-|4\rangle\langle 4|$.

In the case of no relaxation, the convergence behavior for three different values of $\zeta=0.5$, 1.0, and 1.5 is plotted in Fig. 1 when the amplitude parameter, $A=15$. Here, the convergence parameters are assumed to have step-independent values. In Fig. 1, the ordinate shows the logarithm of the difference between the cost functional values at adjacent iteration steps, $\log_{10}[\delta J_{\zeta\eta}^{(k,k-1)}](k=1,2,\ldots)$. The abscissa shows the logarithm of the difference between the cost functional at the $k$th iteration step, $J_{\zeta\eta}^{(k)}$, and the converged value, $J_{\zeta\eta}$, i.e., $-\log_{10}[J_{\zeta\eta}-J_{\zeta\eta}^{(k)}]$. Because of the negative signs in the logarithmic plot, a larger abscissa value means that $J_{\zeta\eta}^{(k)}$ is closer to $J_{\zeta\eta}$. Here, convergence is defined by the value of the cost functional at the final iterative step, beyond

TABLE I. For the results in Fig. 1, a list of the CPU times relative to the Krotov method ($\zeta=1.0$, $\eta=0.0$) and the percentage of the total number of iteration steps required to achieve the specified values of $\delta J_{\zeta\eta}^{(k,k-1)}=10^{-4}$, $10^{-5}$, and $10^{-6}$.

| | $\zeta=0.5$ | $\zeta=1.0$ | $\zeta=1.5$ |
|---|---|---|---|
| $\eta=0.0$ | | | |
| CPU | 0.678 | 1.00 | 1.29 |
| $10^{-4}$ | 76% | 73% | 94% |
| $10^{-5}$ | 93% | 94% | 98% |
| $10^{-6}$ | 98% | 98% | 99% |
| $\eta=0.5$ | | | |
| CPU | 2.94 | 4.12 | 3.12 |
| $10^{-4}$ | 57% | 55% | 48% |
| $10^{-5}$ | 76% | 74% | 64% |
| $10^{-6}$ | 89% | 88% | 80% |
| $\eta=1.0$ | | | |
| CPU | 4.93 | 480 | 737 |
| $10^{-4}$ | 54% | 3.4% | 5.6% |
| $10^{-5}$ | 71% | 49% | 50% |
| $10^{-6}$ | 84% | 76% | 76% |
| $\eta=1.5$ | | | |
| CPU | 5.18 | 13.0 | 26.2 |
| $10^{-4}$ | 53% | 54% | 54% |
| $10^{-5}$ | 72% | 72% | 72% |
| $10^{-6}$ | 86% | 86% | 86% |
| $\eta=2.0$ | | | |
| CPU | 6.41 | 18.6 | 54.6 |
| $10^{-4}$ | 59% | 60% | 60% |
| $10^{-5}$ | 76% | 77% | 77% |
| $10^{-6}$ | 88% | 89% | 90% |

which further monotonic convergence breaks down due to numerical limitations. Reflecting the discrete multiplicity of solutions,[14] each set of convergence parameters may lead to a different solution. In the present example, we see that the converged value of the cost functional virtually does not depend on the convergence parameters since the converged values lie within a narrow range, 0.880 276 ($\zeta=1.5,\eta=0.0$) and 0.881 485 ($\zeta=\eta=1.0$). Actually, the difference in these values is so small that no distinction in pulse shape can be recognized (not shown here), except for a small deviation in the temporal peak position. Physically, these multiple solutions reflect the stationary nature of the present target. That is, the target population stays in the objective state regardless of the time when it is created. In the following analysis, we thus assume that all the parameter sets lead to a physically identical solution.

The results in Fig. 1 are represented by trajectories to easily see the global nature of convergence. They confirm the monotonic convergence behavior of the present algorithm up to high numerical accuracies although the numerical limitations depend on the choice of convergence parameters, $\zeta$ and $\eta$. Several sets of parameters can identify solutions with small intervals, $\delta J_{\zeta\eta}^{(k,k-1)}\leqslant 10^{-10}$. Some trajectories associated with them, however, are temporarily trapped on the way to convergence. Here trapping means that $\delta J_{\zeta\eta}^{(k,k-1)}$ becomes locally small at some value of $k$ far before convergence. From Fig. 1, we also see that the so-called Krotov method[15,16] ($\zeta=1.0,\eta=0.0$) cannot achieve high accuracy compared to other choices of $\zeta$ and $\eta$ values.

Since the trajectory plot does not explicitly reveal information on computational time, Table I shows a list of the CPU times required to achieve convergence, which are given by values relative to the Krotov method ($\zeta=1.0,\eta=0.0$). Table I also shows the number of iteration steps required to achieve specified values of $\delta J_{\zeta\eta}^{(k,k-1)}=10^{-4}$, $10^{-5}$, and $10^{-6}$, given by the percentage of the total number of iteration steps. Comparing relative CPU times to achieve $\delta J_{\zeta\eta}^{(k,k-1)}=10^{-4}$ in cases of ($\zeta=1.0,\eta=0.0$) and ($\zeta=1.0,\eta=0.5$), for example, we have $1.00\times 0.73=0.73$ ($4.12\times 0.55=2.27$) in the former (latter) case. We see that the Krotov method[15,16] usually achieves its convergence limit (although typically of less accuracy than for other sets of $\zeta$, $\eta$ values) with a small number of iteration steps. This appears to be the case, as often a rougher method can achieve convergence with fewer iterations near an optimal solution. We also see in Table I that the case of ($\zeta=0.5,\eta=0.0$) exhibits faster convergence than the Krotov method. Note that in Fig. 1, the trajectories associated with the Krotov method often show fluctuating structures that do not appear with other sets of convergence parameters. This behavior could also be attributed to the rough search nature of the Krotov method.

Another feature is that some sets of parameters which achieve high numerical accuracy also show extremely slow convergence behavior, and such cases are always accompanied by trapping structures in the trajectory. Since we do not have *a priori* knowledge about trapping points, in order to improve computational efficiency we have to restart the calculation with a different set of convergence parameters if the trajectory is trapped.

This situation naturally leads to the question about the choice of "good" parameters. If we are concerned with the fastest convergence, the best parameters are those that maximize an increase in the cost functional difference $\delta J_{\zeta\eta}^{(k,k-1)}$. This maximization condition leads to a set of auxiliary equations as shown in Appendix B. Here we consider a convenient way for choosing the convergence parameters by means of extrapolation. The cost functional difference, $\delta J_{\zeta\eta}^{(k,k-1)}$, can be expressed as

$$\delta J_{\zeta\eta}^{(k,k-1)}=x_k[J_{\zeta\eta}-J_{\zeta\eta}^{(k)}], \tag{21}$$

where the parameter $x_k$ gives an estimate for the roughness of the solution search. We expect that an appropriate value of $x_k$ could be $10^{-3}$–$10^{-1}$. From Eq. (21), we derive

$$\delta J_{\zeta\eta}^{(k,k-1)}=\frac{1}{1+x_k}\left(\frac{x_k}{x_{k-1}}\right)\delta J_{\zeta\eta}^{(k-1,k-2)}, \tag{22}$$

which does not include the unknown converged value, $J_{\zeta\eta}$. Because of $x_k\simeq x_{k-1}$, Eq. (22) gives a good criterion to check the convergence behavior. If the change in the cost functional difference is found to be out of the range specified by $x_k$, then we will continue the calculation but with a different set of convergence parameters. For example, when a switch was made between the two sets of convergence parameters ($\zeta=1.0,\eta=1.0$) and ($\zeta=1.0,\eta=2.0$) according to the criterion specified by $x_k\in[10^{-3},10^{-1}]$, we found that

the convergence trajectory was not trapped, although the numerical accuracy reduced to $-\log_{10}[J_{\zeta\eta}-J_{\zeta\eta}^{(k)}]=9.0$ (not shown here).

Finally, we will briefly discuss the control mechanism using an analytically solvable model. Suppose that the system interacts with the electric field

$$E(t)=E_1(t)+E_2(t)$$
$$=f(t)[E_1^0\cos(\omega_1 t)+E_2^0\cos(\omega_2 t+\theta)], \quad (23)$$

where $f(t)$ is a pulse envelope function, and the central frequencies $\omega_1$ and $\omega_2$ are tuned to the transition frequencies $\varepsilon_{31}$ and $\varepsilon_{43}=\varepsilon_{32}$, respectively. According to the transition moment elements, we introduce two Rabi frequencies $\Omega_1$ and $\Omega_2$ that are, respectively, defined by

$$\hbar\Omega_1=\mu_0 E_1^0, \quad \hbar\Omega_2=\mu_0 E_2^0\exp(-i\theta). \quad (24)$$

Under the RWA, it is easy to solve Schrödinger's equation analytically for an arbitrary initial condition. If the population is initially in state $|1\rangle$ or $|3\rangle$, the pulse in Eq. (23) leads to the same populations for $|2\rangle$ and $|4\rangle$ at any time. However, if the system is initially in the superposition of states $|1\rangle$ and $|3\rangle$ such that

$$|\psi(t=0)\rangle=|1\rangle\cos x+|3\rangle e^{iy}\sin x, \quad (25)$$

the populations of states $|2\rangle$ and $|4\rangle$ are given by

$$P_n(t)=\frac{|\Omega_2|^2}{\Omega^2}\left|(-1)^{n/2+1}\frac{\Omega_1}{\Omega}(1-\cos\Omega\tau)\cos x\right.$$
$$\left.+ie^{iy}\sin\Omega\tau\sin x\right|^2 \quad (n=2,4), \quad (26)$$

where the plus (minus) sign of the first term in $|\cdots|$ corresponds to state $|2\rangle$ ($|4\rangle$). In Eq. (26), $\Omega$ and $\tau$ are defined by

$$\Omega=\sqrt{|\Omega_1|^2+2|\Omega_2|^2}, \quad \tau=\tfrac{1}{2}\int_0^t ds\, f(s), \quad (27)$$

respectively. The different phases in Eq. (26) enable the pulse to selectively excite either state $|2\rangle$ or $|4\rangle$. Based on this analysis, we suggest the following qualitative picture of the control mechanism. In the first step, the optimal pulse creates an appropriate superposition of states, $|1\rangle$ and $|3\rangle$. Then, by adjusting the relative phases, the pulse selectively induces stimulated emission in order to transfer the population to state $|2\rangle$ and prevents the population from being transferred to state $|4\rangle$.

The same calculations were performed in the presence of relaxation processes that are characterized by the phenomenological dephasing parameters, $\gamma_{mn}^{(d)}=\gamma_{nm}^{(d)}=\langle\langle mn|\Gamma|mn\rangle\rangle=0.2$ $(m\neq n)$ except $\gamma_{24}^{(d)}=\gamma_{42}^{(d)}=0.5$. Using the amplitude parameter, $A=30$, we solve the pulse design equations for several sets of convergence parameters, $\zeta$ and $\eta$. The converged values of the cost functional range from 0.427 841 $(\zeta=1.5,\eta=0.0)$ to 0.428 591 $(\zeta=0.5,\eta=0.5)$. All the optimal pulses have similar structures (not shown); they have Gaussian-type shapes with the peak intensities being higher than those in the absence of relaxation in order to quickly establish coherence for achieving control. Their temporal peak positions differ since we are now concerned with a stationary target. In Fig. 2, the convergence trajectories are shown. We see monotonic convergence behavior confirming the formal results in Sec. II. Trapped structures appear when the parameter $\eta$ is set to 1.5 and 2.0. Note that these sets of parameters are different from those causing "trapping" in Fig. 1.

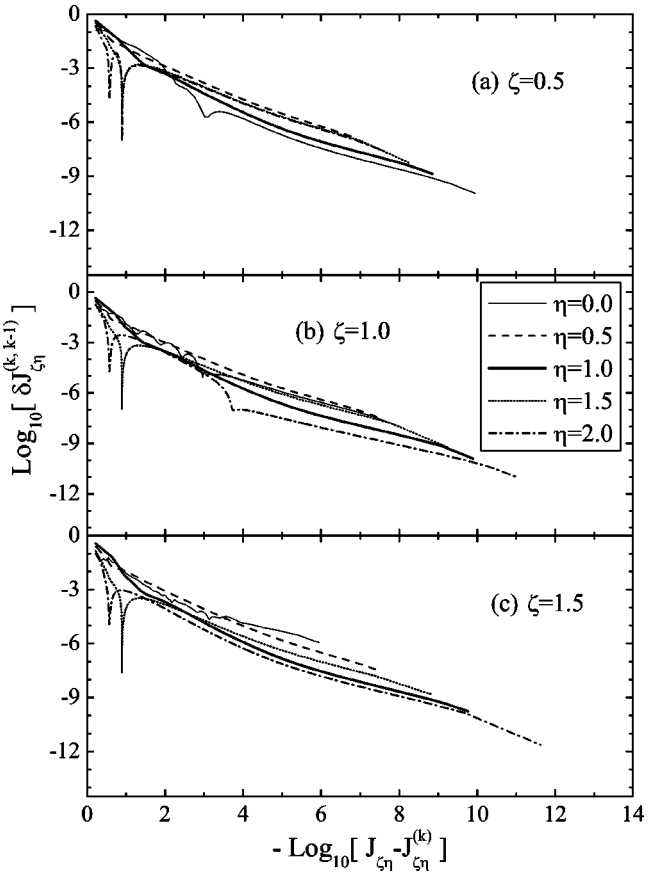


FIG. 2. Global nature of convergence behavior in the presence of relaxation. For the relaxation parameters, see the text. Three values of (a) $\zeta=0.5$, (b) 1.0, and (c) 1.5 are considered.

Table II shows the CPU times relative to the Krotov case of $(\zeta=1.0,\eta=0.0)$. For this set of convergence parameters, the relative CPU times in Table I are approximately two times longer than that in Table II. That is slow convergence when either $\zeta$ or $\eta$ is greater than 1. This behavior may indicate that the structure of the cost functional changes depending on the relaxation conditions. In addition, in Table II, the relative CPU times are distributed within a much narrower range than those in Table I. Although it is not clear if these results are general, they suggest that the presence of relaxation leads to more rapid convergence.

Next, we consider convergence behavior in the case of a nonstationary target using another four-level model, in which the objective state is characterized by a finite lifetime. The energy eigenvalues associated with state $\{|n\rangle\}(n=1,2,3,4)$ are set to $\varepsilon_1=0.0$, $\varepsilon_2=30.0$, $\varepsilon_3=30.5$, and $\varepsilon_4=55.0$, respectively. The transition moment elements are chosen as $\mu_{12}=\mu_{13}=\mu_{24}=-\mu_{34}=\mu_0$, where we assume $\mu_{mn}=\mu_{nm}$. The goal of the control is to achieve the largest transition probability from an initial state $|1\rangle$ to an objective state $|4\rangle$. This objective state is assumed to be coupled with dark states

TABLE II. For the results in Fig 2, a list of the CPU times relative to the Krotov method ($\zeta=1.0$, $\eta=0.0$) and the percentage of the total number of iteration steps required to achieve the specified values of $\delta J_{\zeta\eta}^{(k,k-1)}=10^{-4}$, $10^{-5}$, and $10^{-6}$. The label "n.a." means that the set of convergence parameters cannot achieve the specified numerical accuracy.

| | $\zeta=0.5$ | $\zeta=1.0$ | $\zeta=1.5$ |
|---|---|---|---|
| $\eta=0.0$ | | | |
| CPU | 3.82 | 1.00 | 0.702 |
| $10^{-4}$ | 64% | 77% | 92% |
| $10^{-5}$ | 81% | 91% | 98% |
| $10^{-6}$ | 92% | 97% | n.a. |
| $\eta=0.5$ | | | |
| CPU | 0.321 | 0.479 | 0.577 |
| $10^{-4}$ | 76% | 74% | 72% |
| $10^{-5}$ | 89% | 88% | 87% |
| $10^{-6}$ | 96% | 96% | 95% |
| $\eta=1.0$ | | | |
| CPU | 1.30 | 2.50 | 3.71 |
| $10^{-4}$ | 55% | 53% | 53% |
| $10^{-5}$ | 77% | 75% | 75% |
| $10^{-6}$ | 91% | 90% | 90% |
| $\eta=1.5$ | | | |
| CPU | 4.83 | 17.8 | 42.6 |
| $10^{-4}$ | 97% | 98% | 99% |
| $10^{-5}$ | 99% | 99% | 99% |
| $10^{-6}$ | 100% | 100% | 100% |
| $\eta=2.0$ | | | |
| CPU | 24.3 | 21.0 | 15.9 |
| $10^{-4}$ | 99% | 55% | 78% |
| $10^{-5}$ | 100% | 84% | 89% |
| $10^{-6}$ | 100% | 95% | 96% |

that cause irreversible population relaxation characterized by the parameter $\langle\langle 44|\Gamma|44\rangle\rangle=0.1$. We consider three cases of dephasing, (R1) $\gamma_{kl}^{(d)}=0.1$, (R2) $\gamma_{kl}^{(d)}=0.3$ except $\gamma_{23}^{(d)}=\gamma_{32}^{(d)}=0.1$, and (R3) $\gamma_{kl}^{(d)}=0.5$ except $\gamma_{23}^{(d)}=\gamma_{32}^{(d)}=0.3$. Under those relaxation conditions, we solve the pulse design equations with an amplitude parameter, $A=15$, for three sets of convergence parameters, (a) $(\zeta,\eta)=(1.0,0.0)$, (b) (1.0, 1.0), and (c) (0.5, 1.5). The optimal solutions achieve the transition probabilities, (R1) 64%, (R2) 56%, and (R3) 37%, where we have virtually the same values independent of the choice of convergence parameters.

Figure 3 and Table III show the trajectory plots and the list of relative CPU times, respectively. The trajectories in Fig. 3 clearly show the monotonic convergence behavior of the present algorithms for the nonstationary target. We see that a longer CPU time tends to lead to higher numerical accuracy, in which considerable computational time is sometimes attributed to the iteration steps around a trapping point. There was no trapping under the relaxation condition of (R3). In this example, larger dephasing parameters tend to remove such trapping points.

## IV. SUMMARY

We have developed a family of new monotonically convergent algorithms for solving the pulse design equations. The equations are derived from the two basic functionals that describe a wide range of physical criteria for designing pulses, and are expressed in terms of product-space notation. We have applied those algorithms to a cost functional that is constructed with the aim of achieving the largest transition

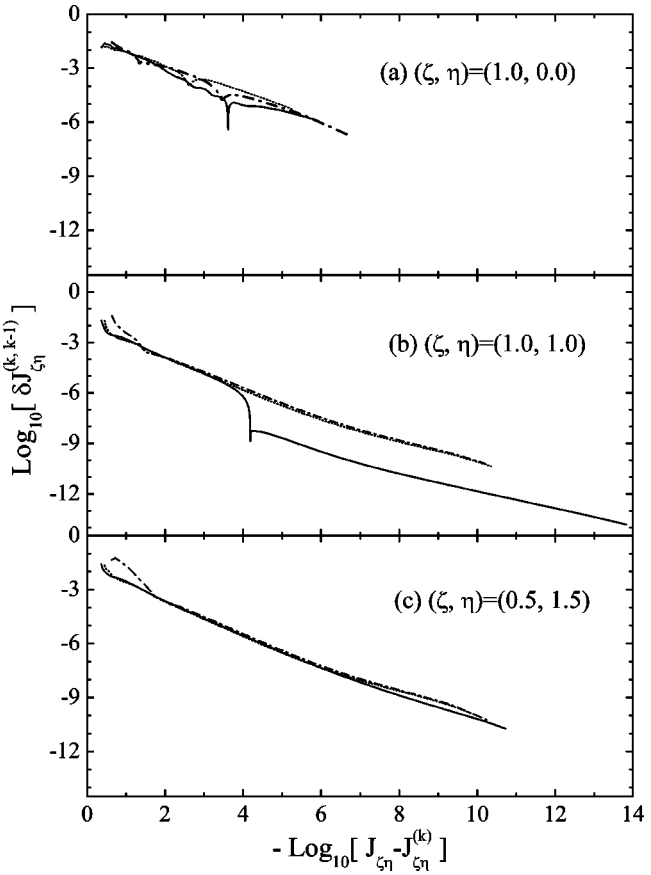


FIG. 3. Global nature of convergence behavior for three sets of convergence parameters, (a) $(\zeta=1.0,\eta=0.0)$, (b) $(\zeta=1.0,\eta=1.0)$, and (c) $(\zeta=0.5,\eta=1.5)$. The solid, dotted, and dot-dashed lines correspond to the results associated with the relaxation conditions of (R1), (R2), and (R3), respectively (see the text).

TABLE III. For the results in Fig. 3, a list of the CPU times relative to the Krotov method ($\zeta=1.0$, $\eta=0.0$) and the percentage of the total number of iteration steps required to achieve the specified values of $\delta J_{\zeta\eta}^{(k,k-1)}=10^{-4}$, $10^{-5}$, and $10^{-6}$. The label "n.a." means that the set of convergence parameters cannot achieve the specified numerical accuracy.

| | $(\zeta=1.0,\ \eta=0.0)$ | $(\zeta=1.0,\ \eta=1.0)$ | $(\zeta=0.5,\ \eta=1.5)$ |
|---|---|---|---|
| Case (R1) | | | |
| CPU | 1.00 | 229 | 3.89 |
| $10^{-4}$ | 89% | 2.0% | 59% |
| $10^{-5}$ | 97% | 44% | 74% |
| $10^{-6}$ | n.a | 72% | 85% |
| Case (R2) | | | |
| CPU | 0.507 | 6.96 | 3.88 |
| $10^{-4}$ | 95% | 62% | 62% |
| $10^{-5}$ | 98% | 77% | 77% |
| $10^{-6}$ | n.a. | 88% | 89% |
| Case (R3) | | | |
| CPU | 0.521 | 5.15 | 2.61 |
| $10^{-4}$ | 88% | 62% | 57% |
| $10^{-5}$ | 95% | 77% | 73% |
| $10^{-6}$ | 98% | 88% | 86% |

probability from an initial state to an objective state subject to minimal pulse fluence. Two four-level models are employed, and the dynamics is described by the optical Bloch equation to include relaxation processes. Numerical results confirm the monotonic convergence behavior of the algorithms for both stationary and nonstationary targets, as well as for several sets of convergence parameters. The convergence behavior is examined using trajectory plots and relative CPU times.

Some sets of convergence parameters achieving high numerical accuracy may suffer from extremely slow convergence, which is attributed to local trapping. In the examples, relaxation processes tended to remove such trapping structures in the search space. Lack of prior knowledge about trapping prevents choosing appropriate convergence parameters in advance. However, we can monitor the convergence behavior by means of extrapolation. Once unfavorable behavior is observed, the calculation can be restarted at a different set of convergence parameters using the electric field found just prior on the trapped trajectory, taking advantage of the flexibility of the algorithms. There are a number of ways to set convergence criteria as well as choose the convergence parameters; these choices should be made in relation to the available computational resources, required numerical accuracies, etc. Such modifications can easily be included in the software.

## ACKNOWLEDGMENTS

Y.O. is grateful to Professor T. Nakajima for helpful suggestions. He also acknowledges support in the form of a Grant-in-Aid for Scientific Research on Priority Areas "Control of Molecules in Intense Laser Fields" from the Ministry of Education, Culture, Sports, Science and Technology (MEXT) of the Japanese Government. G.T. acknowledges financial support from the ACI "Laser control" of the MENRT (France). H.R. would like to acknowledge support from the U.S. Department of Energy.

## APPENDIX A: THE SOLUTION ALGORITHM AND ITS CONVERGENCE BEHAVIOR IN TYPE II CASES

For the pulse design equations derived from the type II functional, the iteration algorithm can be written as

$$i\hbar\frac{\partial}{\partial t}|\lambda^{(k)}(t)\rangle=[\alpha^{\dagger}-\beta^{\dagger}\overline{E}^{(k)}(t)]-i\hbar Y(t)|u^{(k-1)}(t)\rangle, \tag{A1}$$

with a final condition $|\lambda^{(k)}(t_f)\rangle=X|u^{(k-1)}(t_f)\rangle$, and

$$i\hbar\frac{\partial}{\partial t}|u^{(k)}(t)\rangle=[\alpha-\beta E^{(k)}(t)]|u^{(k)}(t)\rangle, \tag{A2}$$

and an initial condition $|u^{(k)}(0)\rangle=|u_0\rangle$, where the expressions for the electric fields are the same as those in the type I case, i.e., Eqs. (11) and (12). As the final condition of the Lagrange multiplier includes the final state of the system at the previous step, the iteration must start with $|u^{(0)}(t)\rangle$ with an initial trial field, $E^{(0)}(t)$. Monotonic convergence can be proved in the same manner as shown in Sec. II. To prove monotonicity, we calculate the deviation of the $k$th and $(k-1)$th cost functional, which is given by

$$\begin{aligned}\delta J_{\mathrm{II}}^{(k,k-1)}&=J_{\mathrm{II}}^{(k)}-J_{\mathrm{II}}^{(k-1)}\\&=\langle\delta u^{(k,k-1)}(t_f)|X|\delta u^{(k,k-1)}(t_f)\rangle\\&\quad+2\,\mathrm{Re}\langle u^{(k-1)}(t_f)|X|\delta u^{(k,k-1)}(t_f)\rangle\\&\quad+\int_0^{t_f}dt\langle\delta u^{(k,k-1)}(t)|Y(t)|\delta u^{(k,k-1)}(t)\rangle\\&\quad+2\,\mathrm{Re}\int_0^{t_f}dt\langle u^{(k-1)}(t)|Y(t)|\delta u^{(k,k-1)}(t)\rangle\\&\quad-\frac{1}{\hbar A}\int_0^{t_f}dt\{[E^{(k)}(t)]^2-[E^{(k-1)}(t)]^2\},\end{aligned} \tag{A3}$$

where $|\delta u^{(k,k-1)}(t)\rangle=|\delta u^{(k)}(t)\rangle-|\delta u^{(k-1)}(t)\rangle$. To evaluate the difference in the control achievement, we introduce a function, $P^{(k,k-1)}(t)=2\,\mathrm{Re}\langle\lambda^{(k)}(t)|\delta u^{(k,k-1)}(t)\rangle$, which has a null value at $t=0$. Differentiating this function with respect to time, we obtain

$$\begin{aligned}&\frac{d}{dt}P^{(k,k-1)}(t)+2\,\mathrm{Re}\langle u^{(k)}(t)|Y(t)|\delta u^{(k,k-1)}(t)\rangle\\&=\frac{2}{\hbar A}\left\{\left[\frac{1}{\zeta_k}E^{(k)}(t)+\left(1-\frac{1}{\zeta_k}\right)\overline{E}^{(k)}(t)\right][E^{(k)}(t)\right.\\&\quad-\overline{E}^{(k)}(t)]+\left[\frac{1}{\eta_k}\overline{E}^{(k)}(t)+\left(1-\frac{1}{\eta_k}\right)E^{(k-1)}(t)\right]\\&\quad\left.\times[\overline{E}^{(k)}(t)-E^{(k-1)}(t)]\right\}.\end{aligned} \tag{A4}$$

Integrating both sides of Eq. (A4) from $t=0$ to $t_f$, the left-hand side of the resulting equation gives the second and fourth terms on the right-hand side of Eq. (A3). We thus rewrite Eq. (A3) as

$$\begin{aligned}\delta J_{\mathrm{II}}^{(k,k-1)}&=\langle\delta u^{(k,k-1)}(t_f)|X|\delta u^{(k,k-1)}(t_f)\rangle\\&\quad+\int_0^{t_f}dt\langle\delta u^{(k,k-1)}(t)|Y(t)|\delta u^{(k,k-1)}(t)\rangle\\&\quad+\frac{1}{\hbar A}\int_0^{t_f}dt\left\{\left(\frac{2}{\zeta_k}-1\right)[E^{(k)}(t)-\overline{E}^{(k)}(t)]^2\right.\\&\quad\left.+\left(\frac{2}{\eta_k}-1\right)[\overline{E}^{(k)}(t)-E^{(k-1)}(t)]^2\right\}.\end{aligned} \tag{A5}$$

The summation of Eq. (A5) from $k=1$ to $N$ leads to $\delta J_{\mathrm{II}}^{(N,0)}\geqslant 0$ for positive definite target operators $X$ and $Y(t)$. This is valid as long as the convergence parameters, $\{\zeta_k\}$ and $\{\eta_k\}$, are within the range [0, 2].

## APPENDIX B: PARAMETER $\zeta$ ACHIEVING THE FASTEST CONVERGENCE FOR $\eta=0$

Convergence parameters that achieve the fastest convergence are defined by those that maximize the increase in the

cost functional difference, $\delta J_j^{(k,k-1)}$ with $j=$I,II. Although the analysis that follows can be done in general, the most important properties can be seen in the case $\eta_k=0$, and thus considering this simpler case is not restrictive. When dealing with the type I case, setting $\eta_k=0$ implies that $\overline{E}^{(k)}=E^{(k-1)}(t)$ resulting in

$$\delta J_{\mathrm{I}}^{(k,k-1)}=\frac{1}{\hbar A}\int_0^{t_f}dt\left(\frac{2}{\zeta_k}-1\right)[E^{(k)}(t)-E^{(k-1)}(t)]^2. \tag{B1}$$

The goal is to optimize this increase with respect to the parameter, $\zeta_k$.

The difference in the cost functional in Eq. (B1) depends not only on $\zeta_k$ but also $|u^{(k)}(t)\rangle$ and $E^k(t)$, which are subjected to the constraints of Eqs. (10) and (12), respectively. These considerations lead to expressing $\delta J_{\mathrm{I}}^{(k,k-1)}$ as a function of $\zeta_k$, $|u^{(k)}(t)\rangle$ and $E^k(t)$, defined by

$$\begin{aligned}\delta J_{\mathrm{I}}^{(k,k-1)}=&\frac{1}{\hbar A}\int_0^{t_f}dt\left(\frac{2}{\zeta_k}-1\right)[E^{(k)}(t)-E^{(k-1)}(t)]^2\\&+\mathrm{Re}\int_0^{t_f}dt\left\langle\Lambda^{(k)}(t)\right|\left\{i\hbar\frac{\partial}{\partial t}|u^{(k)}(t)\rangle\right.\\&\left.-[\alpha+\beta E^{(k)}(t)]|u^{(k)}(t)\rangle\right\}+\int_0^{t_f}dt\,f^{(k)}(t)\\&\times[E^{(k)}(t)-(1-\zeta_k)E^{(k-1)}(t)\\&+\zeta_k A\,\mathrm{Im}\langle\lambda^{(k)}|\beta|u^{(k)}(t)\rangle],\end{aligned} \tag{B2}$$

where the Lagrange multipliers, $|\Lambda^{(k)}(t)\rangle$ and $f^{(k)}(t)$, are introduced to fulfill Eqs. (10) and (12), respectively. At the optimal value of $\zeta_k$, all the partial derivatives of $\delta J_{\mathrm{I}}^{(k,k-1)}$ vanish. By setting to zero the variation of $\delta J_{\mathrm{I}}^{(k,k-1)}$ with respect to $E^k(t)$ and $|u^{(k)}(t)\rangle$, we obtain the following supplementary formulas:

$$\begin{aligned}&\frac{1}{\hbar A}\left(-\frac{2}{\zeta_k^2}\right)\int_0^{t_f}dt[E^{(k)}(t)-E^{(k-1)}(t)]^2+\int_0^{t_f}dt\,f^{(k)}(t)\\&\times[E^{(k-1)}(t)+A\,\mathrm{Im}\langle\lambda^{(k)}|\beta|u^{(k)}(t)\rangle=0,\end{aligned} \tag{B3}$$

$$\begin{aligned}&\frac{2}{\hbar A}\left(\frac{2}{\zeta_k}-1\right)[E^{(k)}(t)-E^{(k-1)}(t)]\\&-\mathrm{Re}\langle\Lambda^{(k)}(t)|\beta|u^{(k)}(t)\rangle+f^{(k)}(t)=0,\end{aligned} \tag{B4}$$

and

$$\begin{aligned}i\hbar\frac{\partial}{\partial t}|\Lambda^{(k)}(t)\rangle=&[\alpha^\dagger+\beta^\dagger E^{(k)}(t)]|\Lambda^{(k)}(t)\rangle\\&-if^{(k)}(t)\zeta_k A\beta^\dagger|\lambda^{(k)}(t)\rangle\end{aligned} \tag{B5}$$

with a final condition $|\Lambda^{(k)}(t_f)\rangle=0$. Note that Eq. (B4) easily allows for obtaining the expression for $f^{(k)}(t)$. Substituting the resulting equation into Eq. (B3) and then utilizing the relation

$$\begin{aligned}&\frac{[E^{(k)}(t)-E^{(k-1)}(t)]}{\zeta_k}\\&=-E^{(k-1)}(t)-A\,\mathrm{Im}\langle\lambda^{(k)}(t)|\beta|u^{(k)}(t)\rangle\end{aligned} \tag{B6}$$

we obtain

$$\begin{aligned}&2(\zeta_k-1)\int_0^{t_f}dt\left[\frac{E^{(k)}(t)-E^{(k-1)}(t)}{\zeta_k}\right]^2\\&=-\hbar A\int_0^{t_f}dt\,\mathrm{Re}\langle\Lambda^{(k)}|\beta|u^{(k)}(t)\rangle\left[\frac{E^{(k)}(t)-E^{(k-1)}(t)}{\zeta_k}\right].\end{aligned} \tag{B7}$$

Several update formulas for $\zeta_{k+1}$ can be proposed at this point, for instance:

$$\zeta_{k+1}=1+\frac{\theta}{\nu}, \tag{B8}$$

but also

$$\zeta_{k+1}=\frac{\nu}{\nu-\theta\zeta_k}, \tag{B9}$$

where

$$\nu=2\int_0^{t_f}dt\left[\frac{E^{(k)}(t)-E^{(k-1)}(t)}{\zeta_k}\right]^2, \tag{B10}$$

and

$$\theta=-\hbar A\int_0^{t_f}dt\,\mathrm{Re}\langle\Lambda^{(k)}|\beta|u^{(k)}(t)\rangle\left[\frac{E^{(k)}(t)-E^{(k-1)}(t)}{\zeta_k}\right]. \tag{B11}$$

These formulas are to be understood in the sense that if the quantity given by Eq. (B8) or (B9) has a value less than zero it is set to zero, and if it has a value larger than 2 it is set to 2.

In another approach to update $\zeta_k$, we use $g_k$, the gradient of $\delta J_{\mathrm{I}}^{(k,k-1)}$ with respect to $\zeta_k$,

$$g_k=\frac{\delta J_{\mathrm{I}}^{(k,k-1)}}{\zeta_k}=2(\zeta_k-1)\nu-\theta. \tag{B12}$$

We then have an update formula

$$\zeta_{k+1}=\zeta_k+\rho_k g_k,\quad \rho_k>0, \tag{B13}$$

where $\rho_k$ is chosen such that $\zeta_{k+1}\in[0,2]$.

In the same way, we can derive the formulas in the type II case. That is, by setting the variation of $\delta J_{\mathrm{II}}^{(k,k-1)}$ with respect to its arguments, we obtain the three equations, two of which are the same as those in the type I case, Eqs. (B3) and (B4). For the equation of motion for the Lagrange multiplier, $|\Lambda^{(k)}(t)\rangle$, we have

$$\begin{aligned}i\hbar\frac{\partial}{\partial t}|\Lambda^{(k)}(t)\rangle=&[\alpha^\dagger+\beta^\dagger E^{(k)}(t)]|\Lambda^{(k)}(t)\rangle-if^{(k)}(t)\\&\times\zeta_k A\beta^\dagger|\lambda^{(k)}(t)\rangle-2Y(t)|\delta u^{k,k-1}(t)\rangle\end{aligned} \tag{B14}$$

with a final condition $|\Lambda^{(k)}(t_f)\rangle=(2/i\hbar)X|\delta u^{(k,k-1)}(t_f)\rangle$. The update formulas are the same as before [Eqs. (B8) and (B9)], where $\nu$ and $\theta$ are given by Eqs. (B10) and (B11), respectively.

[1] H. Rabitz, R. de Vivie-Riedle, M. Motzkus, and K. Kompa, Science **288**, 824 (2000).

[2] H. Rabitz, G. Turinici, and E. Brown in *Computational Chemistry* edited by Ph. G. Ciarlet, Special Volume of Handbook of Numerical Analysis Vol X, edited by C. Le Bris (Elsevier Science, Amsterdam, 2003), p. 833.
[3] Y. Ohtsuki and H. Rabitz, CRM Proceedings and Lecture Notes **33**, 151 (2003).
[4] G. Turinici and Y. Maday, Proceedings of the 41st CDC IEEE Conference, 2002, p. 1364.
[5] Y. Maday and G. Turinici, J. Chem. Phys. **118**, 8191 (2003).
[6] C. Le Bris, Y. Maday, and G. Turinici, CRM Proceedings and Lecture Notes **33**, 127 (2003).
[7] W. Zhu, J. Botina, and H. Rabitz, J. Chem. Phys. **108**, 1953 (1998).
[8] W. Zhu and H. Rabitz, J. Chem. Phys. **109**, 385 (1998).
[9] Y. Ohtsuki, W. Zhu, and H. Rabitz, J. Chem. Phys. **110**, 9825 (1999).
[10] Y. Ohtsuki, J. Chem. Phys. **119**, 661 (2003).
[11] Y. Ohtsuki, K. Nakagami, Y. Fujimura, W. Zhu, and H. Rabitz, J. Chem. Phys. **114**, 8867 (2001).
[12] K. Blum, *Density Matrix Theory and Applications* (Plenum, New York, 1981).
[13] Y. Ohtsuki, K. Nakagami, W. Zhu, and H. Rabitz, Chem. Phys. **287**, 197 (2003).
[14] M. Demiralp and H. Rabitz, Phys. Rev. A **47**, 809 (1993).
[15] J. Somlói, V. A. Kazakov, and D. J. Tannor, Chem. Phys. **172**, 85 (1993).
[16] A. Bartana, R. Kosloff, and D. J. Tannor, J. Chem. Phys. **106**, 1435 (1997).